Contrib Mineral Petrol (2001) 141: 643–658
DOI 10.1007/s004100100266

Othmar Müntener · Peter B. Kelemen · Timothy L. Grove

The role of H_2O during crystallization of primitive arc magmas under uppermost mantle conditions and genesis of igneous pyroxenites: an experimental study

Received: 31 October 2000 / Accepted: 1 March 2001 / Published online: 18 May 2001

Abstract Exposed, subduction-related magmatic arcs commonly include sections of ultramafic plutonic rocks that are composed of dunite, wehrlite, and pyroxenite. In this experimental study we examined the effects of variable H_2O concentration on the phase proportions and compositions of igneous pyroxenites and related ultramafic plutonic rocks. Igneous crystallization experiments simulated natural, arc magma compositions at 1.2 GPa, corresponding to conditions of the arc lower crust. Increasing H_2O concentration in the liquid changes the crystallization sequence. Low H_2O concentration in the liquid stabilizes plagioclase earlier than garnet and amphibole while derivative liquids remain quartz normative. Higher H_2O contents ($>3\%$) suppress plagioclase and lead to crystallization of amphibole and garnet thereby producing derivative corundum normative andesite liquids. The experiments show that alumina in the liquid correlates positively with Al in pyroxene, as long as no major aluminous phase crystallizes. Extrapolation of this correlation to natural pyroxenites in the Talkeetna and Kohistan arc sections indicates that clinopyroxenes with low Ca-Tschermaks component represent near-liquidus phases of primitive, Si-rich hydrous magmas.

Density calculations on the residual solid assemblages indicate that ultramafic plutonic rocks are always denser than upper mantle rocks in the order of 0.05 to 0.20 g/cm^3. The combination of high pressure and high H_2O concentration in the liquid suppresses plagioclase crystallization, so that ultramafic plutonic rocks form over a significant proportion of the crystallization interval (up to 50% crystallization of ultramafic rocks from initial, mantle-derived liquids). This suggests that in subduction-related magmatic arcs the seismic Moho might be shallower than the petrologic crust/mantle transition. It is therefore possible that calculations based on seismic data have overestimated the normative plagioclase content (e.g., SiO_2, Al_2O_3) of igneous crust in arcs.

O. Müntener (✉) · P.B. Kelemen
Department of Geology and Geophysics,
Woods Hole Oceanographic Institution,
Woods Hole, MA 02543, USA

O. Müntener · T.L. Grove
Department of Earth, Atmospheric and Planetary Sciences,
Massachusetts Institute of Technology,
Cambridge, MA 02139, USA

Present address: O. Müntener
Institut de Géologie, Université de Neuchâtel,
CH-2007 Neuchâtel, Switzerland
e-mail: Othmar.Muentener@unine.ch
Tel.: +41-32-7182659, Fax: +41-32-7182601

Editorial responsibility: J. Hoefs

Introduction

Constraints on the origin and evolution of island arc crust are crucial in understanding the genesis of continents. Agreement exists that the most significant factor in increase of the volume of the continental crust since the Archean has been the accretion of island arcs along convergent plate boundaries. In fact, geochemical data suggest that arc magmatism was the major factor in the formation of Archean continental crust as well (e.g., Rudnick 1995). Mass balance estimates of the bulk composition of exposed island arc sections yield a basaltic bulk composition (DeBari and Sleep 1991; Miller and Christensen 1994) consistent with the observation that basalts are the most abundant, primitive lavas along present-day convergent margins. However, estimates of the bulk continental crust show an andesitic composition (e.g., Rudnick and Fountain 1995; Taylor and McLennan 1985). A variety of reasons have been put forward to explain this apparent paradox (Kelemen 1995; Rudnick and Fountain 1995).

Ultramafic plutonic rocks play a key role in addressing this issue as their physical properties such as density and seismic velocity are very similar to residual upper mantle peridotites (Miller and Christensen 1994). Ultramafic plutonic rocks intruding residual mantle

peridotite are commonly found in peridotite massifs and in mantle xenoliths. Wehrlites and pyroxenites are also common in zoned, ultramafic-felsic arc plutons (summary in Kelemen and Ghiorso 1986; Table 6). Very similar wehrlite and pyroxenite xenoliths are common in xenoliths within Aleutian arc magmas (e.g., Conrad and Kay 1984). In addition, hundreds of meters to kilometer-thick igneous pyroxenites are found at the base of exposed island arc sections in the Talkeetna area (Alaska; DeBari and Coleman 1989), the Kohistan region (Pakistan; Miller and Christensen 1994) and Cabo Ortegal (Galicia, NW Spain; Girardeau et al. 1989). In fact, we are not aware of any exposed arc Moho section which does not include pyroxenite sections between overlying crustal gabbroic rocks and underlying residual mantle peridotite. Pyroxenites at the base of arc sections have several features indicating crystallization from primitive magmas. In particular, they have high Mg#, and relatively high Cr, but comparatively low Na and Al contents. These rocks may contain important clues about the primary magmas that pass from the mantle to form igneous, arc crust.

A major difficulty in studying the genesis of high Mg# pyroxenites at the base of exposed arc sections is that, at temperatures greater than about 1,050 °C (Holloway and Burnham 1972), hydrous minerals are not stable on the liquidus of primitive arc magmas. As such it is difficult to constrain the H_2O content of magmas that formed ultramafic plutonic rocks. Breakdown of hydrous phases fluxes the overlying mantle wedge with H_2O, causing or enhancing partial melting beneath arcs. Thus, it is crucial to understand the role of H_2O in arc magmatism. The influence of H_2O on mantle melting has been studied by Kushiro (1990), Hirose and Kawamoto (1995), and Gaetani and Grove (1998). In contrast, the influence of H_2O on crystallization of arc magmas in the uppermost mantle and at the crust-mantle boundary is not well understood.

In this paper we explore the effects of variable bulk composition, including H_2O content, on the phase proportions and mineral compositions in igneous pyroxenites. Our approach utilizes water-undersaturated (2.5 to 5 wt%) crystallization experiments on primitive basalts and high Mg# andesites that provide data on the nature of igneous pyroxenites crystallized from hydrous magmas. Comparison of experimental and natural compositions demonstrates that low-Al pyroxene represents a near-liquidus phase in primitive arc-related pyroxenites crystallized from hydrous magmas. The alumina content of pyroxenes at constant pressure is dependent on the Al/Si ratio of the liquid, thus providing a tool to link pyroxenite compositions to parental magmas. Upon crystallization, a variety of ultramafic cumulates are formed (websterite, garnet pyroxenites, garnet-amphibole pyroxenites) before plagioclase saturation occurs. The combination of high pressures (>1.0 GPa) and variable water contents probably are the prime factors in controlling the plagioclase saturation boundary. If voluminous ultramafic cumulates are crystallized from hydrous magmas, this could lead to a discrepancy between the depth of the seismic Moho and the thickness of the igneous crust in arcs. Finally, the densities of experimentally produced, garnet-bearing cumulates are significantly higher than densities of residual mantle peridotite, creating a potentially unstable density inversion.

Experimental techniques

Starting material

Two primitive lavas from the Mt. Shasta region (northern California, USA), a basaltic andesite (85–44) and a high Mg# andesite (85–41) were chosen as the starting material (Table 1). These lavas have Mg#s of 0.71 and 0.74, respectively, and were previously shown to be in equilibrium with mantle harzburgite (Baker et al. 1994) at pressure equivalent to the crust-mantle boundary below Mt. Shasta.

Starting materials consisted of mixes of rock powder and an H_2O saturated glass prepared from the rock powder. In this way, the H_2O content of the starting material could be varied. The hydrous glass was synthesized in a zirconium-hafnium carbide-molybdenum (ZHM) cold seal pressure vessel, using a mixture of CH_4 and Ar as a pressure medium, by melting of ca. 300 mg rock powder and 25 ml distilled H_2O in a gold capsule. The charge was held at 0.2 GPa and 1050 °C for 24 h, after which the experiment was terminated using a rapid quenching technique (Sisson and Grove 1993a). Saturation with H_2O was confirmed by piercing the capsule after the experiment and testing for liquid H_2O. The run products (hydrous glass, olivine, clinopyroxene, spinel) were analyzed with the electron microprobe and the relative proportions of glass and minerals were determined by least squares regression analysis and the bulk H_2O content was calculated. The remaining material was ground under ethanol for at least 1 h; the resulting powder was then used as the initial material for piston cylinder experiments.

Capsule material

Iron loss from the sample to metal capsules can be a serious problem in H_2O undersaturated experiments. In order to minimize Fe loss during our experiments, we pre-saturated the capsule material with Fe using the technique developed by Gaetani and Grove (1998). $Au_{80}Pd_{20}$ capsules were filled with a basaltic powder and held in a vertical gas-mixing furnace at 0.1 MPa and 1,250 °C with fO_2 close to the QFM buffer for 48 h. After quenching, the glass was removed using a warm HF bath for 24 to 48 h. The cleaned, Fe-pre-saturated capsules were then used for piston cylinder experiments.

Table 1 Starting material for high pressure experiments, analyzed and reported by Baker et al. (1994)

Sample	SiO_2	TiO_2	Al_2O_3	FeO	MnO	MgO	CaO	Na_2O	K_2O	P_2O_5	Cr (ppm)	Ni (ppm)	Mg#
85–44	51.68	0.60	16.40	7.93	0.16	10.79	9.67	2.24	0.42	0.11	693	230	0.707
85–41c	57.79	0.60	14.46	5.74	0.11	9.14	8.17	3.11	0.71	0.15	590	121	0.738

Experimental methods

H_2O undersaturated experiments were performed in a 1.27-cm solid medium piston cylinder device (Boyd and England 1960). Experiments at 1.2 GPa were first pressurized to 1.0 GPa at room temperature after which the temperature was raised to 865 °C at 100 °C/min. The pressure was then raised to the desired run pressure and the temperature was held constant for 6 min. Final run temperature was subsequently reached by increasing the temperature at a rate of 50 °C/min. The pressure medium of most runs was sintered $BaCO_3$. Pressure was calibrated by investigating the transition of anorthite, gehlenite and corundum to Ca-tschermakite that is known to be almost T-independent (Hays 1966) and to occur at 1.35 GPa at 1300 °C. The calibration runs showed that no friction correction has to be applied, and therefore the reported pressures are uncorrected. Temperature was monitored by using W-Re thermocouples without correction for the effect of pressure on the thermocouple emf and was controlled to within ±2 °C of the set point using a Eurotherm controller. Temperatures are corrected for the temperature difference (20 °C) between the hotspot and the position of the thermocouple and are probably accurate to within 10 °C.

Experimental assemblies were similar to those used by Gaetani and Grove (1998). Experiments were prepared by packing 6–12 mg of powder into a Fe saturated $Au_{80}Pd_{20}$ capsule that was sealed by arc welding. The capsule was placed into a graphite sleeve, and this in turn was placed into a Pt capsule packed with graphite powder. The welded Pt capsule was fit to an outer, high-density Al_2O_3 sleeve and centered in the hotspot of a straight-wall graphite furnace with MgO spacers. The thermocouple entered the assembly via an aluminium sheath and was separated from the Pt outer capsule by a disk of MgO.

Analytical methods

All experimental run products were analyzed using a 5-spectrometer JEOL 733 electron microprobe at the Massachusetts Institute of Technology. A 10 nA beam current and 15 kV accelerating potential were used for all analyses. Beam diameters were 20 μm for hydrous glasses, and 2 μm for crystalline phases. The hydrous glasses were analyzed for O using the techniques described in Gaetani and Grove (1998). H_2O contents of the glasses were evaluated from the remaining O after calculation of all other oxides (i.e., SiO_2, TiO_2, Al_2O_3, ...). Hydrous basaltic glass secondary standards (87s35a) of Sisson and Grove 1993b) were analyzed at the beginning of each microprobe session to determine the accuracy and reproducibility of the O analyses. An average of 71 analyses of 87s35a provided a calculated H_2O content of 6.08 ± 0.52 wt%, which is in good agreement with H_2O determined by FTIR (5.94 ± 0.17 wt%, Sisson and Grove 1993b). On-line data reduction was accomplished using the CIT-ZAF correction procedure. Analytical precision was estimated from replicate analyses of a basalt glass working standard, and standard deviations are: 1.08% for SiO_2, 1.26% for Al_2O_3, 1.31% for CaO, 1.67% for MgO, 2.4% for FeO, 8.7% for TiO_2, 9.2% for Na_2O, 3.5% for K_2O, 22% for MnO, 67% for Cr_2O_3, and 12% for P_2O_5.

Results

Experimental run conditions, phase assemblages and proportions, Fe/Mg K_d's, and relative iron losses/gains are listed in Table 2. Phase and liquid compositions are reported in Table 3. In all but two runs, two pyroxenes and silicate glass were present. Mass balance calculations show that Fe loss/gain was low (< 10% relative) and therefore a constant bulk composition was closely approximated. Fe-loss or gain is neither related to the capsule mass/sample mass ratio, to run temperature or to the calculated H_2O concentration in the melt (Fig. 1). However, it is suggested that runs with significant amphibole or garnet have lower apparent Fe exchange (< 3%) because least squares regressions to a given bulk rock composition improve as the number of phases present increases.

The mineral/melt Fe-Mg partitioning indicates a close approximation to equilibrium. The average K_d Fe-Mg concentrations in the basalt versus the magnesian andesite (clinopyroxene: 0.30 ± 0.01 versus 0.27 ± 0.01; orthopyroxene: 0.28 ± 0.01 versus 0.28 ± 0.01) are slightly lower than those for peridotite melting experiments (Gaetani and Grove 1998; Robinson et al. 1998). This is probably due to the different bulk compositions. In all experiments with a degree of crystallization higher than 30%, partially reacted or unreacted cores are occasionally present in clinopyroxene. These cores result from the natural rock powder and/or the 0.2 GPa H_2O-saturated synthesis experiments, indicating that complete chemical equilibrium was not achieved. However, rim compositions of clinopyroxene were identical within error, regardless of the composition of the unreacted core in the experiments. This consistency provides an apparent reversal of composition. In reconstructing a mass balance for our experiments, we used rim compositions of clinopyroxene in conjunction with analysis of glasses and other phases (orthopyroxene, amphibole, spinel, garnet, and/or plagioclase), which were generally homogeneous.

In order to determine the location of olivine-orthopyroxene-clinopyroxene saturation boundaries, 5 wt% hydrous Fo_{90} (oxide + brucite mix with a composition of Fo_{90} + 5 wt% H_2O) was added to the 85–44 hydrous glass initial material. In these experiments olivine was the liquidus phase at 1250 °C, joined by clino- and orthopyroxene at 1,230 °C. The fO_2 of olivine-saturated experiments was calculated using the method of Kress and Carmichael (1991), with Fe^{3+} in the liquid obtained from olivine-liquid Fe^{2+} partitioning, and varies between QFM and QFM –1.

All experiments contained a large amount of silicate melt, which quenched to a homogeneous glass with 4.2 ± 0.3 to 9.0 ± 0.2 wt% H_2O (H_2O includes H_2O and probably CO_2. Gaetani and Grove (1998) report CO_2 in hydrous glasses analyzed by FTIR, indicating that Pt and AuPd capsules probably do not behave as inert containers with respect to graphite).Molar Mg numbers (Mg#, calculated assuming all Fe as FeO) in glasses vary from 0.69 to 0.48. The degree of crystallization varied from < 5 to 60%. High-pressure crystal fractionation produced websterite solid assemblages with variable cpx/opx ratios that increase with decreasing temperature and/or with increasing H_2O in the melt. However, the crystallization sequence and phase proportions are strongly dependent on the initial H_2O content (Table 2). Experiments with the lowest H_2O (2.5 wt%) produced websterite at 1,190 °C and

Table 2 Experimental run conditions, phase assemblages and proportions, Fe/Mg K_d's, and relative iron losses/gains. K_d's are calculated as FeO_{sol}*MgO_{liq}/FeO_{liq}*MgO_{sol}. ΔFe is the difference between the FeO content of the bulk initial material and the FeO in the bulk composition as determined by mass balance calculations in relative weight percent. Positive values indicate apparent Fe gain, negative values indicate relative Fe loss. Phase proportions were obtained by least square calculations. Units in parentheses indicate 2τ error from regression analysis. Accordingly, phase proportions 88.9(21) are read as 88.9 ± 2.1

Runs	P (GPa)	T(°C)	(h)	H_2O (melt)	H_2O init (wt%a)	Run products	Phase proportions (wt%)	Kd						Δ Φε (%)	ΣP2	capsule (g)	sample (g)	samp/caps ratio
								Cpx	Opx	OI	Spi	Grt	Am					
Basalt (85-44)																		
B690	1,2	1230	25	4.4(3)	~3.8	Gl, Cpx, Opx	88.9(21):2.8(27):8.2(19)	0,31	0,29					–4,08	0,16	0,1005	0,0089	0,08806
B674	1,2	1190	25	4.2(3)	~3.8	Gl, Cpx, Opx	77.5(25):12.6(30):9.9(21)	0,31	0,29					–0,55	0,22	0,1124	0,0093	0,08230
B659	1,2	1150	22	5.7(7)	~3.8	GI, Cpx, Opx, Spl	65.3(13):20.5(16):14.1(11):tr.	0,28	0,29					–1,88	0,08	0,1212	0,0081	0,06686
B681	1,2	1110	27	5.5(2)	~3.8	GI, Cpx, Opx, Grt, Spi	49.8(14):31.0(16):13.7(12):4.9(19):0.6(5)	0,32	0,29		1,78	0,55		0,38	0,04	0,1059	0,0078	0,07365
B726	1,2	1070	30	6.4(7)	~3.8	Gl, Cpx, Opx, Grt, Am	39.9(19):27.0(43):8.8(23):15.3(51):8.9(24)	0,31	0,29			0,56	0,34	1,79	0,09	0,0832	0,0078	0,09375
B714	1,2	1230	24	5.3(2)	~5	Gl, Cpx, Opx	90.5(38):2.9(26):6.5(33)	0,30	0,30					9,45	0,64	0,0723	0,0060	0,08299
B686	1,2	1210	26	5.6(4)	~5	Gl, Cpx, Opx	88.3(13):4.5(17):7.2(12)	0,28	0,27					1,48	0,07	0,0951	0,0083	0,08728
B671	1,2	1190	26	5.3(6)	~5	Gl, Cpx, Opx	89.6(30):4.1(35):6.3(26)	0,29	0,28					6,81	0,38	0,1151	0,0090	0,07823
B665	1,2	1150	26	6.5(4)	~5	Gl, Cpx, Opx	76.0(36):12.5(40):11.4(29)	0,29	0,28					8,34	0,52	0,1078	0,084	0,07746
B683	1,2	1110	26	6.0(5)	~5	Gl, Cpx, Opx, Spi	61.9(29):23.6(33):13.7(21):1.1(9)	0,30	0,28		0,70			4,20	0,21	0,1158	0,0088	0,07599
B704	1,2	1070	32	9.0(3)	~5	Gl, Cpx, Opx, Grt, Am	46.9(14):19.1(25):10.1(12):0.1(31):23.9(6)	0,30	0,28				0,61 0,33	0,76	0,05	0,1128	0,0080	0,07092
B679	1,2	1190	27	3.5(5)	~2.5	Gl, Cpx, Opx	69.3(35):17.6(46):13.0(31)	0,31	0,29					–8,39	0,49	0,1206	0,0082	0,06799
B668	1,2	1150	28	4.5(5)	−2.5	Gl, Cpx, Opx, Pl	53.3(85):23.5(45):16.2(41):6.9(59)	0,28	0,27					–7,25	0,43	0,1104	0,0104	0,09420
Basalt + 5% hydrous Fo90																		
B725	1,2	1250	22	5.4(2)	−5	Gl, Ol	97.2(11):2.8(9)			0,3				3,92	0,19	0,0915	0,0089	0,09672
B736	1,2	1230	16	5.8(2)	−5	Gl, Ol, Cpx, Opx	83.5(69):8.6(32):7.6(73):0.3(11)	0,31	0,27	0,29				8,25	0,92	0,0939	0,0078	0,08307
High Mg# andesite (85-41c)																		
B706	1,2	1230	26	4.9(4)	−5	Gl, Opx	95.7(14):4.3(12)		0,31					7,08	0,21	0,0873	0,0081	0,09278
B705	1,2	1190	25	6.1(2)	−5	Gl, Cpx, Opx	88.0(7):4.8(8):7.2(6)	0,28	0,29					–2,75	0,03	0,1130	0,0094	0,08319
B702	1,2	1150	25	5.5(4)	−5	Gl, Cpx, Opx	79.5(20):10.8(28):9.7(20)	0,27	0,29					–5,12	0,30	0,1164	0,0097	0,08333
B707	1,2	1110	28	7.2(8)	−5	Gl, Cpx, Opx	71.9(18):16.5(24):11.6(19)	0,26	0,28					4,01	0,25	0,0950	0,0097	0,10211
B708	1,2	1070	32	7.0(8)	−5	Gl, Cpx, Opx	62.1(14):23.9(21):14.0(16)	0,27	0,26					5,76	0,18	0,0893	0,0085	0,09518
B720	1,2	1030	42	8.8(6)	−5	Gl, Cpx, Opx	63.2(17):22.1(25):14.7(19)	0,26	0,29					1,45	0,27	0,0823	0,0078	0,09478

Table 3 Electron microprobe analyses of run products. Al Fe as FeO. Units in parentheses indicate standard deviation (2τ) from average analysis. Accordingly 2.84(13) should be read as 2.84 ± 0.13

Run Nr.	Phase	Analyses	SiO_2	TiO_2	Al_2O_3	Cr_2O_3	FeO*	MnO	MgO	CaO	Na_2O	K_2O	P_2O_5	NiO	H_2O	Total
B690	Liquid	13	50.0 (2)	0.56 (2)	17.0 (1)	0.04 (1)	7.22 (13)	0.17 (4)	8.21 (9)	9.47 (6)	2.84 (13)	0.38 (2)	0.17 (2)	< 0.01	4.4 (3)	100,5
	Cpx	12	52.8 (3)	0.18 (2)	4.7 (5)	0.91 (10)	4.9 (3)	0.13 (3)	18.6 (4)	17.9 (6)	0.50 (2)					100,7
	Opx	11	55.0 (7)	0.08 (3)	4.1 (7)	0.67 (15)	7.7 (2)	0.13 (4)	30.9 (4)	1.91 (10)	0.06 (2)					100,5
B674	Liquid	11	50.9 (3)	0.62 (2)	18.0 (1)	0.04 (1)	7.61 (14)	0.11 (3)	6.83 (8)	8.67 (9)	3.30 (9)	0.49 (2)	0.22 (9)	0.06 (2)	4.2 (3)	101,0
	Cpx	14	51.8 (5)	0.28 (4)	7.1 (6)	0.45 (11)	5.9 (2)	0.15 (3)	17.2 (4)	17.9 (4)	0.57 (4)					101,4
	Opx	8	52.6 (3)	0.1 (2)	7.0 (5)	0.33 (8)	9.5 (3)	0.17 (2)	29.0 (4)	1.51 (11)	0.06 (3)					100,2
B659	Liquid	14	49.9 (4)	0.63 (2)	19.7 (2)	< 0.01	7.02 (17)	0.14 (2)	5.10 (8)	7.82 (8)	3.7 (2)	0.50 (2)	0.17 (2)	< 0.01	5.7 (4)	100,4
	Cpx	6	49.9 (6)	0.41 (5)	8.0 (8)	0.36 (11)	6.1 (2)	0.15 (2)	15.7 (7)	18.5 (6)	0.58 (5)					99,7
	Opx	8	51.4 (2)	0.20 (2)	7.9 (4)	0.20 (8)	10.8 (2)	0.19 (2)	27.1 (2)	1.48 (15)	0.06 (2)					99,3
	Spinel	5	0.11 (6)	0.18 (4)	62.1 (13)	0.87 (26)	18.4 (8)	0.13 (2)	16.9 (4)	0.16 (3)						99,0
B681	Liquid	4	53.0 (1)	0.69 (2)	19.9 (1)	< 0.01	5.62 (19)	0.09 (4)	3.42 (12)	6.34 (7)	3.96 (17)	0.69 (2)	0.18 (3)	0.05 (3)	5.5 (2)	99,5
	Cpx	13	48.0 (8)	0.62 (8)	10.4 (9)	0.09 (5)	7.3 (4)	0.16 (2)	13.8 (5)	17.6 (9)	0.82 (6)					98,8
	Opx	8	50.1 (5)	0.19 (3)	9.0 (9)	0.09 (7)	12.0 (3)	0.17 (3)	25.6 (1)	1.27 (9)	0.09 (3)					98,6
	Garnet	16	40.4 (2)	0.37 (5)	22.9 (12)	0.22 (6)	13.3 (3)	0.40 (4)	14.8 (2)	6.9 (2)	< 0.01					99,3
B726	Liquid	12	56.5 (4)	0.60 (3)	19.0 (1)	< 0.01	4.31 (15)	0.06 (2)	2.5 (3)	5.2 (3)	4.95 (13)	0.80 (3)	0.18 (1)	< 0.01	6.4 (7)	100,4
	Cpx	9	49.3 (4)	0.57 (7)	9.5 (6)	0.13 (6)	7.4 (5)	0.11 (2)	13.8 (3)	18.4 (5)	0.99 (11)					100,1
	Opx	1	52,7	0,19	7,51	0,02	12,2	0,05	23,9	1,44	0,18					98,2
	Garnet	15	40.3 (5)	0.66 (17)	22.7 (5)	0.16 (8)	14.1 (4)	0.35 (6)	14.5 (4)	7.5 (6)	0.02 (2)					100,2
	Hbl	11	42.4 (6)	1.7 (3)	15.7 (4)	0.20 (11)	8.8 (3)	0.04 (2)	15.0 (3)	10.2 (2)	2.98 (9)	0.29 (2)				97,3
B714	Liquid	11	48.5 (2)	0.59 (2)	16.5 (1)	0.07 (1)	8.2 (3)	0.15 (3)	8.50 (6)	9.41 (11)	2.81 (11)	0.39 (3)	0.19 (2)	0.05 (2)	5.3 (2)	100,6
	Cpx	9	52.9 (8)	0.15 (2)	3.4 (5)	0.74 (14)	5.4 (3)	0.15 (5)	18.8 (6)	17.5 (7)	0.42 (7)					99,5
	Opx	10	54.4 (9)	0.08 (2)	3.5 (6)	0.71 (16)	8.6 (5)	0.16 (3)	30.1 (5)	1.94 (11)	0.05 (2)					99,6
B686	Liquid	11	49.1 (3)	0.55 (2)	17.0 (1)	0.03 (2)	7.68 (18)	0.17 (3)	8.06 (9)	9.23 (9)	2.83 (15)	0.37 (1)	0.17 (2)	< 0.01	5.6 (4)	100,7
	Cpx	14	53.3 (4)	0.12 (1)	3.2 (3)	0.63 (6)	5.3 (4)	0.16 (2)	20.2 (7)	17.2 (9)	0.46 (3)					100,6
	Opx	8	54.6 (7)	0.07 (2)	3.8 (6)	0.77 (15)	7.9 (2)	0.16 (2)	31.3 (5)	1.86 (8)	0.08 (3)					100,5
B671	Liquid	10	48.8 (3)	0.60 (2)	16.5 (1)	0.05 (2)	8.05 (9)	0.11 (4)	8.3 (1)	9.15 (14)	2.85 (12)	0.42 (2)	0.14 (3)	0.05 (2)	5.3 (6)	100,3
	Cpx	12	53.3 (7)	0.17 (3)	3.8 (8)	0.62 (13)	5.5 (4)	0.16 (3)	19.2 (7)	17.6 (9)	0.44 (4)					100,6
	Opx	10	54.2 (5)	0.07 (2)	4.6 (6)	0.74 (14)	8.3 (2)	0.15 (1)	30.7 (3)	1.81 (8)	0.03 (1)					100,5
B665	Liquid	10	48.2 (2)	0.64 (1)	18.4 (1)	0.01 (1)	8.2 (2)	0.11 (2)	6.4 (1)	8.6 (1)	3.2 (2)	0.47 (2)	0.17 (2)	< 0.01	6.5 (4)	100,9
	Cpx	14	51.7 (4)	0.27 (5)	6.1 (4)	0.52 (13)	6.2 (3)	0.15 (2)	16.7 (5)	19.1 (5)	0.54 (5)					101,3
	Opx	11	53.6 (4)	0.11 (1)	5.7 (3)	0.44 (11)	10.1 (3)	0.18 (2)	29.1 (5)	1.54 (7)	0.06 (2)					100,8
B683	Liquid	11	49.2 (7)	0.68 (2)	18.8 (3)	0.02 (2)	7.06 (12)	0.15 (3)	4.5 (1)	7.09 (14)	3.53 (21)	0.57 (2)	0.14 (2)	0.05 (3)	6.0 (5)	97,7
	Cpx	13	48.7 (5)	0.47 (8)	8.4 (8)	0.12 (5)	6.76 (13)	0.13 (2)	14.4 (4)	18.6 (3)	0.70 (5)					98,4
	Opx	8	51.1 (5)	0.15 (2)	6.8 (6)	0.11 (8)	11.6 (3)	0.17 (1)	26.6 (3)	1.22 (16)	0.06 (2)					97,9
	Spinel	9	0.22 (2)	0.18 (2)	62.4 (11)	0.67 (38)	18.2 (6)	0.13 (3)	17.0 (2)	0.17 (4)				0.22 (4)		99,2
B704	Liquid	5	53.6 (3)	0.45 (4)	19.2 (3)	< 0.01	5.5 (3)	0.10 (4)	2.9 (3)	6.27 (18)	3.61 (19)	0.57 (4)	0.15 (2)	< 0.01	9.0 (3)	101,3
	Cpx	12	48.7 (5)	0.44 (6)	9.1 (7)	0.11 (7)	7.8 (2)	0.13 (4)	13.8 (3)	18.8 (6)	0.81 (4)					99,6
	Opx	8	51.6 (3)	0.11 (2)	6.8 (4)	0.12 (6)	13.7 (4)	0.19 (5)	26.4 (6)	1.07 (10)	0.08 (2)					100,1
	Garnet	11	41.2 (3)	0.36 (7)	23.3 (3)	0.21 (11)	15.3 (4)	0.49 (7)	13.4 (3)	7.5 (2)	< 0.01					101,7
	Hbl	10	41.8 (4)	1.22 (6)	16.4 (2)	0.27 (9)	9.2 (3)	0.14 (2)	14.8 (3)	10.5 (1)	2.76 (8)	0.28 (2)				97,5
B679	Liquid	11	51.2 (3)	0.63 (4)	19.4 (2)	< 0.01	6.8 (2)	0.16 (3)	5.9 (1)	8.42 (8)	3.54 (18)	0.48 (2)	0.18 (3)	< 0.01	3.5 (5)	100,2
	Cpx	13	49.8 (5)	0.38 (5)	8.3 (5)	0.38 (6)	5.8 (3)	0.16 (4)	16.0 (2)	17.6 (7)	0.67 (5)					99,1
	Opx	8	51.7 (4)	0.15 (3)	7.5 (2)	0.34 (7)	9.37 (12)	0.18 (3)	28.1 (5)	1.72 (5)	0.08 (4)					99,2
B668	Liquid	12	52.7 (3)	0.77 (3)	19.5 (2)	0.03 (2)	6.6 (2)	0.11 (3)	4.3 (3)	7.5 (2)	3.97 (14)	0.65 (4)	0.15 (3)	0.04 (2)	4.5 (5)	100,9
	Cpx	13	50.0 (6)	0.49 (10)	8.5 (6)	0.24 (6)	7.1 (3)	0.18 (4)	16.3 (9)	16.9 (8)	0.70 (8)					100,4
	Opx	10	51.5 (5)	0.19 (2)	8.2 (4)	0.18 (3)	11.3 (3)	0.19 (3)	27.4 (2)	1.64 (21)	0.07 (3)					100,6
	Plag	9	51.7 (8)		30.8 (5)		0.76 (16)		0.21 (5)	13.4 (6)	3.8 (3)	0.1 (3)				100,8
B725	Liquid	12	49.3 (3)	0.52 (2)	14.9 (1)	0.09 (1)	7.74 (18)	0.15 (2)	10.9 (2)	8.71 (9)	2.45 (6)	0.35 (2)	0.13 (2)	< 0.01	5.4 (2)	100,5
	Ol	15	40.3 (3)	< 0.01	0.06 (6)	0.07 (1)	10.4 (2)	0.12 (3)	48.2 (8)	0.16 (2)				0.01 (1)		99,4

Table 3 (Contd.)

Run Nr.	Phase	Analyses	SiO_2	TiO_2	Al_2O_3	Cr_2O_3	FeO*	MnO	MgO	CaO	Na_2O	K_2O	P_2O_5	NiO	H_2O	Total
B736	Liquid	12	48.4 (3)	0.61 (3)	17.1 (1)	0.05 (2)	7.96 (7)	0.06 (2)	7.92 (9)	9.13 (6)	3.00 (14)	0.41 (3)	0.30 (23)	0.01 (1)	5.8 (2)	100,6
	Ol	12	40.1 (5)	< 0.01	0.04 (1)	0.04 (2)	13.2 (8)	0.14 (3)	46.1 (5)	0.18 (2)				0.06 (2)		99,8
	Cpx	11	52.3 (7)	0.20 (3)	4.90 (7)	0.48 (10)	5.5 (3)	0.13 (2)	17.9 (7)	18.1 (10)	0.48 (3)					100,0
	Opx	12	54.3 (5)	0.09 (2)	4.1 (2)	0.69 (16)	8.1 (3)	0.13 (2)	30.6 (4)	1.87 (12)	0.06 (2)					100,0
B706	Liquid	11	54.4 (3)	0.56 (3)	14.1 (1)	0.03 (2)	5.93 (12)	0.14 (4)	7.5 (1)	7.77 (7)	3.10 (18)	0.73 (3)	0.15 (2)	< 0.01	4.9 (4)	99,2
	Opx	12	56.5 (6)	0.07 (3)	1.6 (2)	0.58 (13)	7.7 (3)	0.12 (3)	31.5 (2)	1.66 (6)	0.07 (2)					99,9
B705	Liquid	14	54.5 (3)	0.60 (3)	15.1 (1)	0.01 (1)	5.29 (17)	0.13 (3)	6.15 (7)	7.53 (9)	3.36 (15)	0.79 (2)	0.14 (4)	< 0.01	6.1 (2)	99,7
	Cpx	14	54.0 (3)	0.15 (3)	2.5 (3)	0.58 (10)	4.5 (2)	0.11 (5)	18.5 (5)	19.3 (4)	0.49 (3)					100,0
	Opx	11	56.0 (3)	0.09 (2)	2.0 (3)	0.38 (4)	7.9 (3)	0.13 (3)	31.9 (3)	1.67 (5)	0.07 (2)					100,1
B702	Liquid	13	55.6 (5)	0.63 (2)	16.2 (2)	0.02 (2)	4.94 (15)	0.11 (2)	4.61 (6)	6.80 (4)	3.38 (18)	0.86 (4)	0.17 (2)	0.06 (3)	5.5 (4)	98,8
	Cpx	10	53.5 (6)	0.19 (5)	2.9 (3)	0.48 (13)	5.08 (13)	0.14 (3)	17.7 (4)	19.2 (4)	0.49 (4)					99,6
	Opx	10	55.4 (8)	0.10 (3)	2.2 (4)	0.24 (9)	9.3 (3)	0.15 (4)	30.4 (4)	1.59 (10)	0.02 (2)					99,3
B707	Liquid	14	56.4 (5)	0.64 (4)	17.1 (1)	< 0.01	4.84 (18)	0.11 (2)	3.34 (22)	6.06 (13)	3.65 (19)	0.96 (5)	0.16 (2)	< 0.01	7.2 (8)	100,4
	Cpx	12	52.6 (6)	0.31 (6)	4.3 (5)	0.37 (11)	6.3 (2)	0.11 (3)	16.5 (6)	19.1 (4)	0.65 (4)					100,2
	Opx	9	54.1 (3)	0.14 (2)	3.6 (2)	0.35 (8)	11.5 (6)	0.16 (4)	28.4 (4)	1.45 (13)	0.06 (2)					99,7
B708	Liquid	10	58.0 (7)	0.62 (2)	18.2 (2)	0.01 (1)	3.93 (14)	0.05 (3)	2.08 (28)	5.13 (18)	4.19 (22)	1.09 (5)	0.24 (2)	< 0.01	7.0 (8)	100,5
	Cpx	13	50.6 (8)	0.52 (8)	6.7 (9)	0.28 (17)	7.5 (6)	0.13 (4)	14.9 (6)	18.6 (10)	0.81 (9)					99,9
	Opx	9	52.1 (5)	0.19 (3)	6.1 (5)	0.22 (4)	12.8 (7)	0.16 (4)	26.5 (5)	1.36 (22)	0.06 (1)					99,5
B720	Liquid	7	57.7 (6)	0.63 (4)	18.2 (2)	< 0.01	3.48 (19)	0.04 (3)	1.98 (14)	5.27 (10)	3.88 (16)	1.03 (6)	0.16 (2)	< 0.01	8.8 (6)	101,1
	Cpx	11	51.1 (9)	0.56 (11)	5.6 (8)	0.36 (24)	6.9 (5)	0.17 (3)	15.0 (7)	18.6 (7)	0.74 (6)					99,1
	Opx	7	52.6 (5)	0.23 (2)	4.9 (3)	0.28 (8)	13.2 (2)	0.22 (4)	26.3 (3)	1.27 (10)	0.04 (2)					99,0

gabbronorite at 1,150 °C. Runs with intermediate H_2O (3.8 wt%) produced websterite at 1,230 and 1,190 °C, spinel-websterite at 1,150 °C, and garnet pyroxenite at 1,110 °C followed by garnet-amphibole pyroxenite at 1,070 °C. Runs with the highest concentration of H_2O (about 5%) crystallized websterite at 1,230, 1,190, 1,150 °C and spinel websterite at 1,110 °C. At 1,070 °C, abundant amphibole and minor garnet formed. A comparison of the two 1,070 °C experiments demonstrates the importance of H_2O concentration on the proportions of amphibole and garnet; in otherwise similar bulk compositions, amphibole was more abundant in runs with higher H_2O content.

Discussion

Liquid lines of descent at high pressure

Most of the H_2O undersaturated experiments at 1.2 GPa produced basaltic to andesitic liquids saturated with two pyroxenes ± spinel and, at more than 40% crystallization, garnet and amphibole. Liquid lines of descent are simplified by recalculating melt compositions into mineral end member components (olivine, silica, clinopyroxene, plagioclase) after the method of Grove et al. (1982) and projecting them onto the ternary diagram olivine-diopside-silica (Fig. 2). Crystallization of SiO_2-poor phases (amphibole, spinel, garnet) at constant pressure (1.2 GPa) drives the resulting melt compositions towards the opx-qtz join. For basaltic andesite (Fig. 2a), the composition of the liquid changes from olivine to quartz ± corundum normative, while in the andesite bulk composition (Fig. 2b), liquids are always quartz normative and become corundum normative at a high degree of crystallization. The multiple saturation boundary in Fig. 2b is slightly curved, indicating increasing proportions of clinopyroxene crystallization with respect to orthopyroxene at decreasing temperature.

Corundum normative compositions have previously been reported from hydrous experiments in simple and natural systems (Kushiro and Yoder 1972; Sisson and Grove 1993a) and are not uncommon in calc-alkaline andesites. Gill (1981) summarized the chemical composition of andesites worldwide and found that about 15% are corundum normative. Explanations for the origin of corundum normative liquids in calc-alkaline magma series have varied from pelite assimilation to hornblende fractionation at low pressures (Gill 1981, and references therein).

One parameter critical for understanding the origin of natural, corundum-normative liquids is the depth (i.e., pressure) at which SiO_2 enrichment in derivative liquids occurs. At 2 kbar and H_2O-saturated conditions, Sisson and Grove (1993a) have experimentally shown that the proportion of plagioclase is reduced relative to Fe, Mg silicates in the crystallizing assemblage and spinel stability is enhanced relative to the Fe, Mg silicate

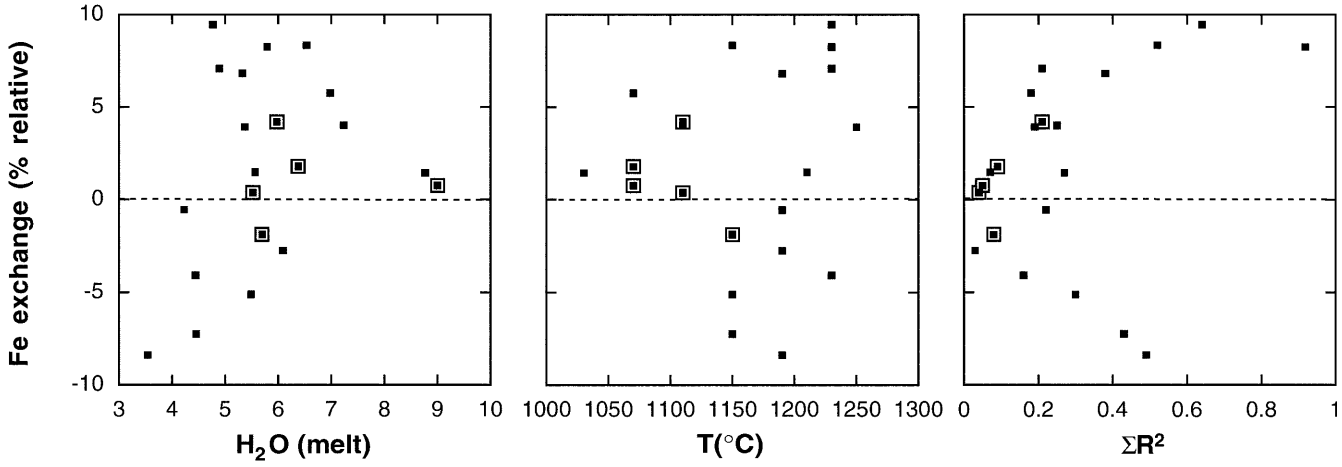

Fig. 1 Relative Fe-loss (in %) in experimental charges. *Large symbols* indicate experimental runs with plagioclase, garnet and/or amphibole present in addition to two pyroxenes

minerals in hydrous basalts (see also Helz 1973; Holloway and Burnham 1972; Kelemen et al. 1990). Grove and Baker (1984) and Grove and Kinzler (1986) emphasized that fractionation at elevated pressure was one important control on the development of the calc-alkaline trend which would cause crystallization of higher proportions of Fe,Mg silicates and a lesser proportion of plagioclase during early stages of differentiation. Our high pressure, H_2O-undersaturated experiments illustrate that plagioclase is suppressed at upper mantle conditions and that SiO_2-poor phases like spinel, garnet and amphibole are stable closer to the liquidus than plagioclase. At pressures corresponding to the base of island arc crust, an increase in SiO_2 is caused by the appearance of garnet + amphibole + spinel as crystallizing phases. Our data support the hypothesis of Kushiro and Yoder (1972) and Cawthorn and Brown (1976), that high H_2O contents in calc-alkaline liquids are a prerequisite for the generation of peraluminous igneous rocks, leaving amphibole and/or garnet-bearing residues in the deep crust.

Clinopyroxene compositions

To investigate the effects of hydrous, high-pressure crystallization on pyroxene composition, the experimentally produced clinopyroxenes were recalculated into the end-member components wollastonite, enstatite + ferrosillite and CaTs + CrTs ($CaCrAlSiO_6$), (plotted in Fig. 3a). Near-liquidus clinopyroxene has low CaTs + CrTs and is similar to clinopyroxene compositions from the 200 MPa, H_2O-saturated experiments carried out by Gaetani et al. (1993). Crystal fractionation increases the CaTs component and decreases the Wo component unless a major Al phase (plagioclase, garnet, amphibole) crystallized. The increase in CaTs + CrTs is caused by the combined effects of high H_2O in the melt and high pressure, which suppress plagioclase and permit enrichment of alumina in residual liquids. In contrast, early plagioclase saturation in both anhydrous and hydrous liquids at lower pressure inhibits an increase in alumina in pyroxenes and liquid with increasing differentiation.

The ternary diagram in Fig. 3b compares clinopyroxene in websterite, garnet websterite and gabbronorite from arc plutonic complexes formed at 1.0 to 1.5 GPa (Kohistan, Talkeetna, Cabo Ortegal: DeBari and

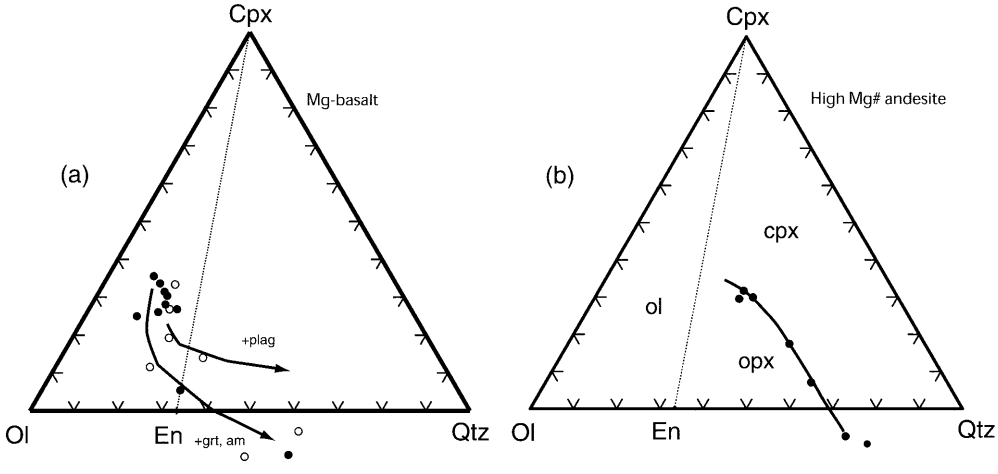

Fig. 2 Pseudo-ternary projections and schematic liquid lines of descent of experimental liquids produced in H_2O undersaturated conditions at 1.2 GPa. **a** Liquids from experiments on basaltic andesite 85–44; **b** liquids from high Mg# andesite 85–41c. Projection scheme is from Grove et al. (1993). Black dots: experoments with 5 wt% H_2O, grey dots: experiments with 3.8 wt% H_2O, open circles: experiments with 2.5 wt% H_2O

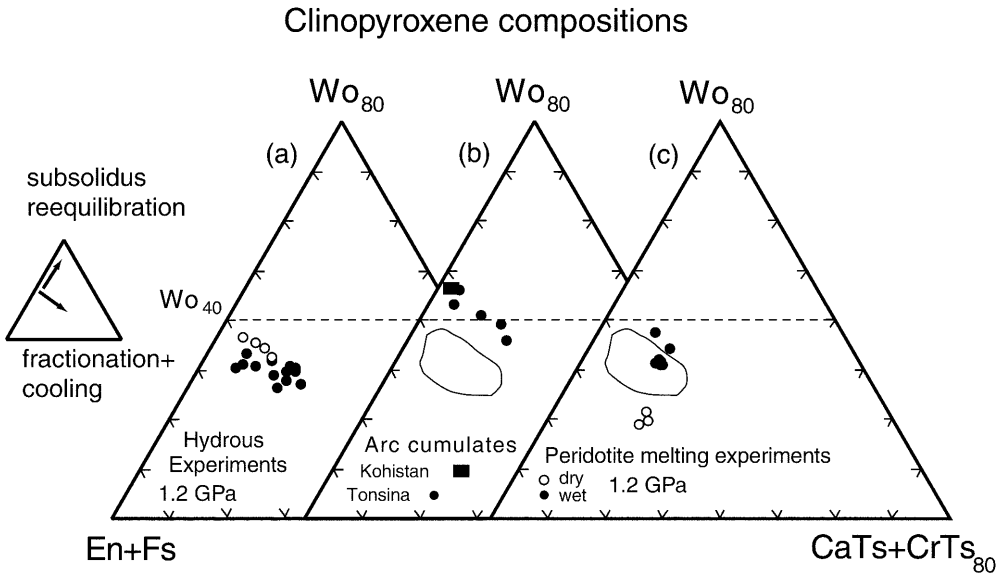

Fig. 3 Clinopyroxene composition recalculated into end member components Wollastonite (Wo) – Enstatite + Ferrosilite (En + Fs) – Al- and Cr-Tschermaks (CaTs + CrTs). **a** Experimental results at 1.2 GPa; *open symbols* high Mg# andesite, *solid circles* basaltic andesite. **b** Pyroxenes in websterites and gabbronorites from the Kohistan and Tonsina arcs (DeBari and Coleman 1989; Jan and Howie 1981). **c** Pyroxenes produced in experiments on olivine-spinel-two pyroxene saturated liquids at 1.2 GPa are from Gaetani and Grove (1998). The field in **b** and **c** covers experiments from this study

Coleman 1989; Gravestock 1992; Jan and Howie 1981) with our high pressure, experimental pyroxenes. Decreasing Wo contents and increasing CaTs + CrTs contents with increasing differentiation characterize the clinopyroxenes from the Tonsina complex. A similar observation was made in our experiments, except that the Tonsina trend is shifted towards generally higher Wo contents. This offset to higher Wo is due to slow cooling of deep-seated, arc plutonic rocks that permitted pyroxenes to reequilibrate to lower temperature, i.e., the immiscibility gap between enstatite and diopside increases. Pyroxene exsolutions and thermobarometric results for websterites, garnet gabbros and gabbronorites reported by DeBari and Coleman (1989) indicate subsolidus equilibration below 900 °C. However, subsolidus equilibration is not expected to change the Al content of pyroxenes significantly, as diffusion rates for Al are orders of magnitudes lower than for Ca-Mg (Sautter et al. 1988).

In Fig. 3c, experimentally produced clinopyroxene compositions coexisting with a four-phase mantle assemblage at 1.2 GPa (Gaetani and Grove 1998) are plotted and compared to the crystallization experiments. Addition of H_2O to the experiments increases the Wo content at similar CaTs + CrTs contents. The lower temperatures at which the hydrous experiments were performed primarily cause the higher Wo content. The CaTs + CrTs content is buffered by the presence of olivine + Cr-spinel, respectively. From these comparisons it is concluded that the major effect of H_2O is to decrease the temperature of crystallization and therefore drive the clinopyroxene composition to higher Wo contents. A low CaTs + CrTs content is indicative of near-liquidus pyroxene crystallization in the absence of an Al phase (i.e., plagioclase, garnet, spinel, hornblende). A similar conclusion can be drawn by comparing 1 atm dry data and 200 MPa H_2O-saturated data of the same composition (Bartels et al. 1991; Sisson and Grove 1993a).

Al partitioning between pyroxene and liquids

Figure 4 shows a plot of Al partitioning between pyroxenes and melt (log D^{Al}) versus reciprocal temperature. In all but three experiments, Al in clinopyroxene exceeds that of coexisting orthopyroxene. The partitioning is approximately linear with reciprocal temperature. The basalt data with different H_2O contents define two, parallel trends, with a third trend defined by the high Mg# andesite data. Experiments with lower bulk

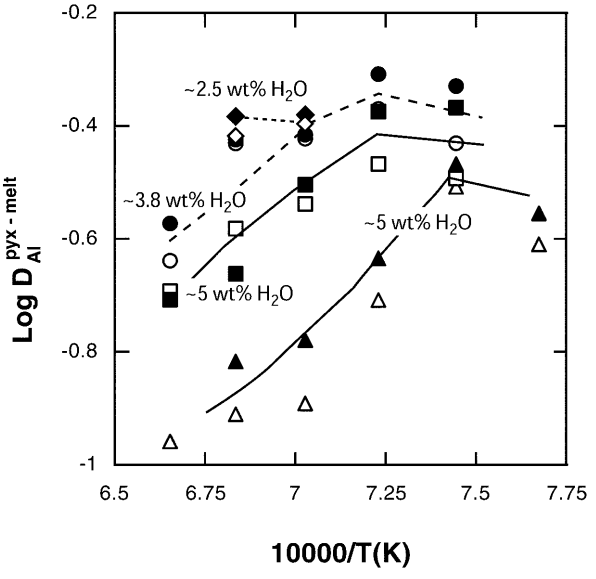

Fig. 4 Al-partitioning between pyroxene and melt versus reciprocal temperature for basaltic andesite (*diamonds*, *squares* and *circles*) and high Mg#-andesite (*triangles*). *Open symbols* are orthopyroxenes, *filled symbols* are clinopyroxenes. An approximately linear correlation exists between D's and reciprocal temperature up to the first appearance of an aluminous phase, after which the D's remain constant. Lines connect experiments with similar bulk H_2O content

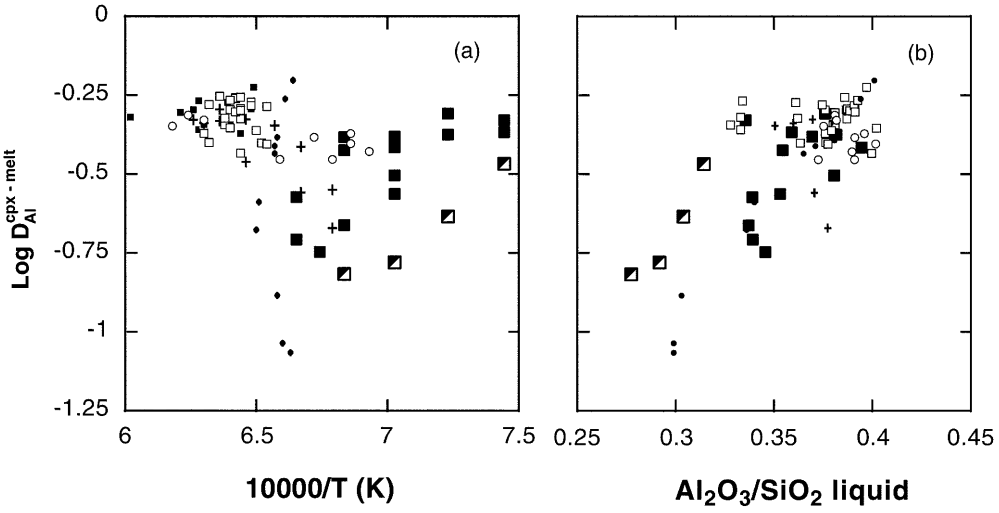

Fig. 5 Al partitioning between clinopyroxene and melt versus reciprocal temperature **a** and versus the ratio Al_2O_3/SiO_2 in the liquid **b**. Sources of data: *filled* (basalt) and *half-filled squares* (high Mg# andesite): this study; *open squares* Kinzler and Grove (1992) and Bartels et al. (1991); *crosses* Draper and Johnston (1992), *full circles* Gaetani and Grove (1995); *open circles* Gaetani and Grove (1998); *small full squares* Robinson et al. (1998). See text for discussion

H_2O show higher partition coefficients at a given temperature. Positive correlations between Al partitioning (pyroxene/melt) and reciprocal temperature hold for assemblages without major Al phases, i.e., any garnet, spinel, plagioclase, or amphibole. This indicates that pyroxenes with a low CaTs component represent near-liquidus phases of primitive magmas ranging from high MgO basalt to high Mg# andesite.

The two contrasting effects of temperature and composition are illustrated in Fig. 5, in which experimental data from this study are compared to other experiments dealing with clino- and orthopyroxene compositions. Mantle melting studies in the spinel-lherzolite field between 1.0 and 1.5 GPa (e.g., Gaetani and Grove 1998; Hirose and Kawamoto 1995; Kinzler and Grove 1992; Robinson et al. 1998) provide partition coefficients between 0.35 and 0.5 and show no systematic variation with temperature (Fig. 5a). Partition coefficients in anhydrous crystallization experiments on a primitive basalt are negatively correlated with reciprocal temperature, an effect that is most likely caused by the high amounts of plagioclase (i.e., low temperature runs of Draper and Johnston 1992), and is the opposite of the trend observed in our experiments. We attribute this to plagioclase crystallization in dry systems, which forces derivative liquids to lower Al contents and also to lower clinopyroxene-melt K_d's.

There is a positive correlation between the $Al^{cpx\text{-}melt}$ partitioning and the Al/Si ratio of the coexisting liquid (Fig. 5b) for experimental runs without coexisting Al phases (garnet, spinel, amphibole, plagioclase). This correlation is mainly defined by our data but is consistent with 1 atm experiments in simple systems (Gaetani and Grove 1995). With the formation of significant garnet and/or hornblende, the Al/Si ratio decreases at D_{Al} comparable to spinel lherzolite melting experiments (Fig. 5b). The lowest D_{Al} has been found for liquids with high H_2O and/or low Al/Si ratios. Figure 6 illustrates a schematic representation of the Di-CaTs join for different Al/Si ratios in the liquid. A low Al/Si ratio in the

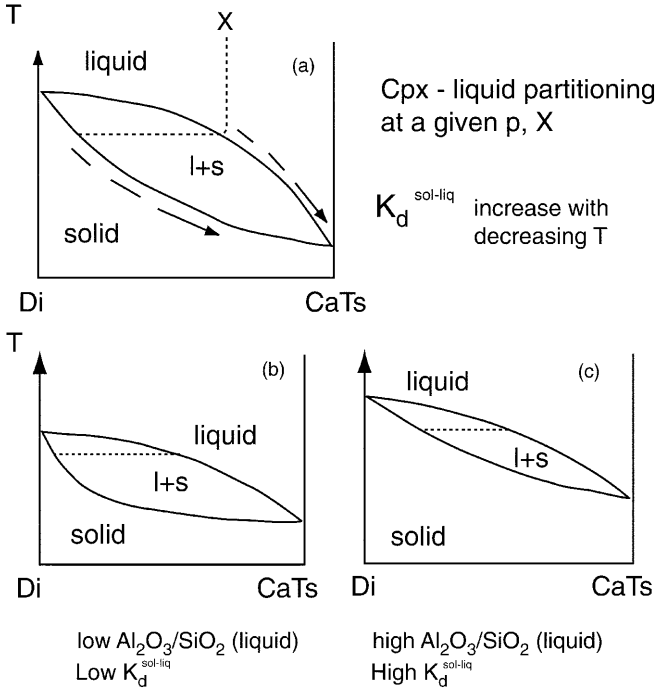

Fig. 6 Schematic representations of the diopside-Ca-Tschermaks (Di-CaTs) join. **a** At a given pressure and composition the $K_d^{sol-liq}$ increases with decreasing temperature. **b** For low Al_2O_3/SiO_2 ratios in the liquid, the Di-CaTs join is broadened and partition coefficients are low. **c** For higher Al_2O_3/SiO_2 ratios the Di-CaTs join is narrower, resulting in higher partition coefficients

liquid broadens the Di-CaTs join, with the consequence that the liquidus clinopyroxene of a hydrous, low Al/Si liquid is extremely low in CaTs compared to liquids with a higher Al/Si ratio and/or less magmatic H_2O. Primitive, two pyroxene-saturated arc magmas with such low Al/Si are high Mg#-andesites and boninites. Picrites also have a low Al/Si ratio; however, they are not saturated in orthopyroxene. Fractional crystallization experiments of a hydrous picrite at 1.0 GPa lead to extensive olivine fractionation and produce spinel-bearing websterites

(pyroxene Mg# of about 0.8; Kägi, personal communication) with high D_{Al}, comparable to the spinel-websterite from run B683. On the other hand, crystallization of a dry tholeiite would saturate early in plagioclase and late in orthopyroxene. Low Al websterite will not be formed in this way. For these reasons, the low Al contents of pyroxenes in websterites from the base of arc crust (Cabo Ortegal, Gravestock 1992) ; Tonsina, DeBari and Coleman 1989) indicate that they crystallized from primitive, hydrous Si-rich liquids.

Residual solid assemblages: websterites and garnet websterites

To compare compositions of arc pyroxenites with our experimental solid assemblages, we calculated experimental bulk solid compositions from the compositions and proportions reported in Table 3. However, please note that we considered the experimental solid compositions as pure adcumulates, neglecting any intercumulus liquid. Table 4 lists these calculated, bulk solid compositions together with selected calculated densities. In Fig. 7 they are compared to pyroxenites from lower crustal arc complexes from Kohistan, Tonsina and Cabo Ortegal. Equilibrium crystallization of basaltic compositions causes an increase in Al_2O_3 and a decrease in SiO_2 in the solid composition at decreasing Mg# (Figs. 7a, b). There are small differences between the experimentally produced pyroxenites and those crystallized at the base of arc crust. The compositions of the latter are partially shifted to higher Mg# at a given SiO_2 content, perhaps reflecting combined crystal fractionation and reaction with surrounding, ultramafic rocks (e.g., Burg et al. 1998; Kelemen 1986; Kelemen and Ghiorso 1986). In Fig. 7c the Cr content of igneous pyroxenites is plotted together with the experimental solid compositions. Natural data agree well with the experimental results, indicating that websterites in arc complexes are formed from primitive magmas with high Cr.

Density calculations on ultramafic plutonic rocks

For experimental runs covering the observed range of solid compositions, densities of the solid assemblages were calculated using the phase equilibrium program Vertex (Connolly 1990) and the thermodynamic database of Holland and Powell (1998), using an interface and plotting software developed by Dr. Matthew Jull at Woods Hole. All calculations were done for the system Na_2O, FeO, CaO, MgO, Al_2O_3, SiO_2 (NFCMAS). We excluded K_2O and TiO_2 from the calculations due to their small abundance in ultramafic plutonic rocks and their incompatibility. We also excluded Cr_2O_3 because currently available pyroxene solution models do not incorporate Cr_2O_3. Finally, the exclusion of H_2O seems justified, as only two experiments involved amphibole

Table 4 Experimental solid compositions calculated from mineral proportions and compositions listed in Tables 2 and 3. Density of residual solids (ρ^{exp}) are calculated from phase proportions and compositions. Density differences ($\delta\rho$) between residual solids and thermodynamic calculations are negligible for spinel websterite and gabbronorite, but larger for websterite and garnet websterite

Sample	Residual solids	SiO_2	TiO_2	Al_2O_3	Cr_2O_3	FeO*	MnO	MgO	CaO	Na_2O	K_2O	Cr ppm	Mg#	ρ^{exp} (g/cm^3)	$\delta\rho^{exp\text{-}calc}$
B659	Spinel Websterite	50.71	0.33	8.00	0.29	8.06	0.16	20.46	11.62	0.37	0.00	2000	0.819	3.335	< 0.02
B665	Websterite	52.05	0.20	5.86	0.48	7.97	0.16	22.38	10.60	0.31	0.00	3256	0.833		
B668	Gabbronorite	50.50	0.31	11.73	0.18	7.53	0.16	17.53	11.08	0.95	0.02	1261	0.806	3.238	< 0.02
B671	Websterite	53.54	0.11	4.22	0.69	7.12	0.15	26.00	7.98	0.19	0.00	4724	0.867		
B674	Websterite	51.70	0.20	6.97	0.40	7.42	0.16	22.19	10.62	0.34	0.00	2709	0.842		
B679	Websterite	51.09	0.29	8.03	0.36	7.36	0.17	2.134	10.94	0.42	0.00	2488	0.838		
B681	Garnet Websterite	48.43	0.48	11.36	0.11	9.33	0.19	17.40	12.15	0.54	0.00	720	0.770	3.370	–0.02
B683	Spinel Websterite	49.07	0.35	9.55	0.14	8.97	0.15	19.20	12.11	0.46	0.00	939	0.792		
B686	Websterite	53.80	0.09	3.53	0.71	6.88	0.16	26.89	7.72	0.22	0.00	4865	0.875		
B690	Websterite	54.11	0.11	4.22	0.73	6.93	0.13	27.65	5.95	0.17	0.00	4992	0.877		
B704	Hbl-Garnet websterite	46.76	0.74	12.10	0.19	9.68	0.15	16.87	11.83	1.56	0.13	1273	0.756		
B714	Websterite	54.18	0.10	3.50	0.72	7.69	0.16	26.71	6.77	0.16	0.00	4921	0.861		
B726	Garnet-Hbl websterite	46.73	0.71	13.56	0.13	10.06	0.15	15.72	11.96	0.93	0.04	910	0.736		
B702	Websterite	54.67	0.15	2.56	0.37	7.10	0.15	23.81	10.93	0.27	0.00	2530	0.857		
B705	Websterite	55.16	0.11	2.17	0.46	6.54	0.12	26.50	8.70	0.24	0.00	3168	0.878	3.260	+0.04
B706	Websterite	56.62	0.07	1.63	0.59	7.72	0.12	31.52	1.67	0.07	0.00	4008	0.879		
B707	Websterite	53.17	0.24	4.00	0.37	8.44	0.13	21.42	11.82	0.41	0.00	2500	0.819		
B708	Websterite	51.28	0.40	6.47	0.26	9.46	0.14	19.23	12.23	0.54	0.00	1777	0.784		

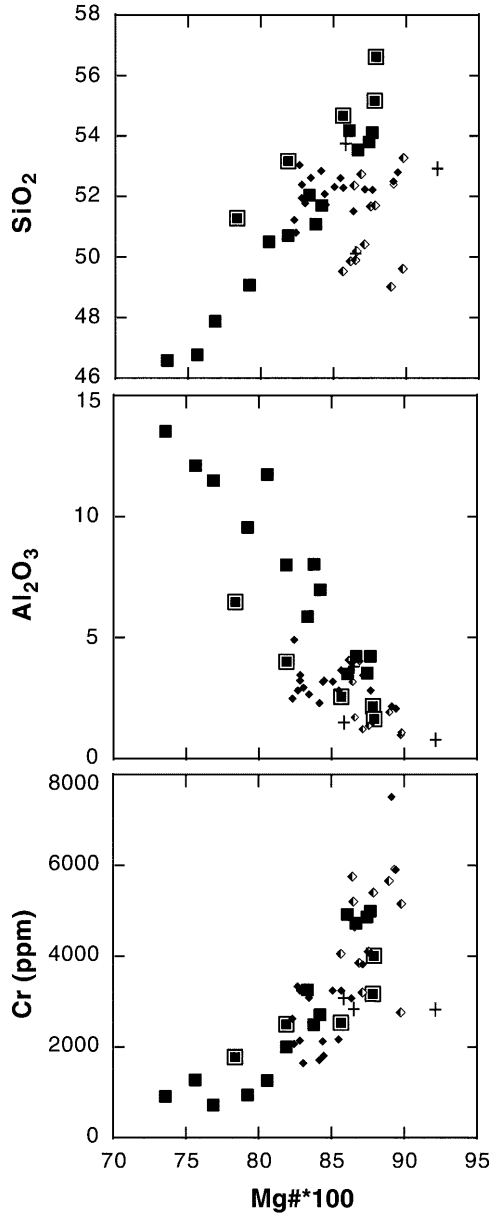

Fig. 7 Chemical composition of igneous pyroxenites from arcs compared to experimental solid assemblages (*squares* basaltic andesite, *squares surrounded by lines* high Mg# andesite) presented in Table 4. Sources of data: Cabo Ortegal: *filled diamonds* (Gravestock 1992); Kohistan: *crosses* (Jan and Howie 1981); Tonsina: *half-filled diamonds* (DeBari and Coleman 1989; S. DeBari, personal communication, 1999)

and the density of igneous amphiboles is comparable to that of clinopyroxene. Phase assemblages were calculated at P and T down to 800 °C, and then densities for lower temperatures using the phase assemblages at (P, 800 °C) and the compressibility of the minerals.

Table 4 lists calculated densities for selected residual solid compositions and density differences between residual solids and those calculated with the thermodynamic database of Holland and Powell (1998) at the P and T conditions of the respective experiments. We find excellent correspondence between experimentally derived and thermodynamically calculated densities for the spinel-websterite and gabbronorite. However, larger differences exist for the orthopyroxene-rich websterite and the garnet pyroxenite (Table 4). There are two important caveats to this comparison: (1) we excluded Cr_2O_3 from the thermodynamic calculations, which results in an overestimate of the stability of olivine and garnet compared to spinel and pyroxenes. This could explain why the opx-rich websterite has a lower, and the garnet-pyroxenite has a higher density in the thermodynamic calculations compared to the density from the residual solid compositions. (2) We have ignored the potential effects of intercumulus liquid (which is probably small). Supposing in an extreme case that 5% trapped liquid (crystallized as granite with a density of 2.7 g/cm^3) was present in sample B659, the calculated density would be reduced by about ~0.03 g/cm^3 This would be in the same range as uncertainties introduced by applying the simple NFCMAS system and would therefore not significantly change the overall results.

Figure 8 shows contours of density calculated for four different experimental solid compositions listed in Table 4 as a function of pressure and temperature. The results show that the density varies from ~3.25 g/cm^3 for websterites to ~3.40 g/cm^3 for garnet-websterites under the experimental conditions (i.e., 1.2 GPa and the respective temperature, Table 2). At a given pressure, the density increase upon cooling is more gradual for the orthopyroxene-rich websterite than for the garnet pyroxenite. Figure 8c, d are density contours for solid bulk compositions produced at the same pressure, temperature, and anhydrous bulk composition (T = 1,150 °C, P = 1.2 GPa), but at different H_2O contents. It is clear that small amounts of plagioclase (15% in run B668) are sufficient to significantly reduce the density of the solid composition.

The density contrast between ultramafic plutonic rocks and underlying mantle (abyssal peridotite: Dick 1989) has been obtained by calculating the density difference at a given pressure and temperature and is illustrated in Fig. 9. For the gabbronorite (Fig. 9d), the maximum density difference is about 0.05 g/cm^3. For the orthopyroxene-rich websterite (Fig. 9b), there is a negligible density contrast with the peridotite. For the pyroxenites (Fig. 9c), a maximum density contrast of about 0.1 g/cm^3 is calculated. For the garnet pyroxenites (Fig. 9a), the maximum density contrast is about 0.15 g/cm^3. As plagioclase crystallization at lower crustal pressures is critically dependent on the H_2O content of melt, it is clear that hydrous magmas have a higher potential to form dense ultramafic plutonic rocks at lower crustal conditions than dry magmas.

As expected, the density contrast between lower crust and mantle is largest for the experimental solid compositions including garnet. The densest of these crystallized at intermediate H_2O contents at 1110 °C (Fig. 9a). At higher H_2O contents, more amphibole and less garnet forms, limiting the calculated density contrast to lower values. At lower H_2O contents, plagioclase is

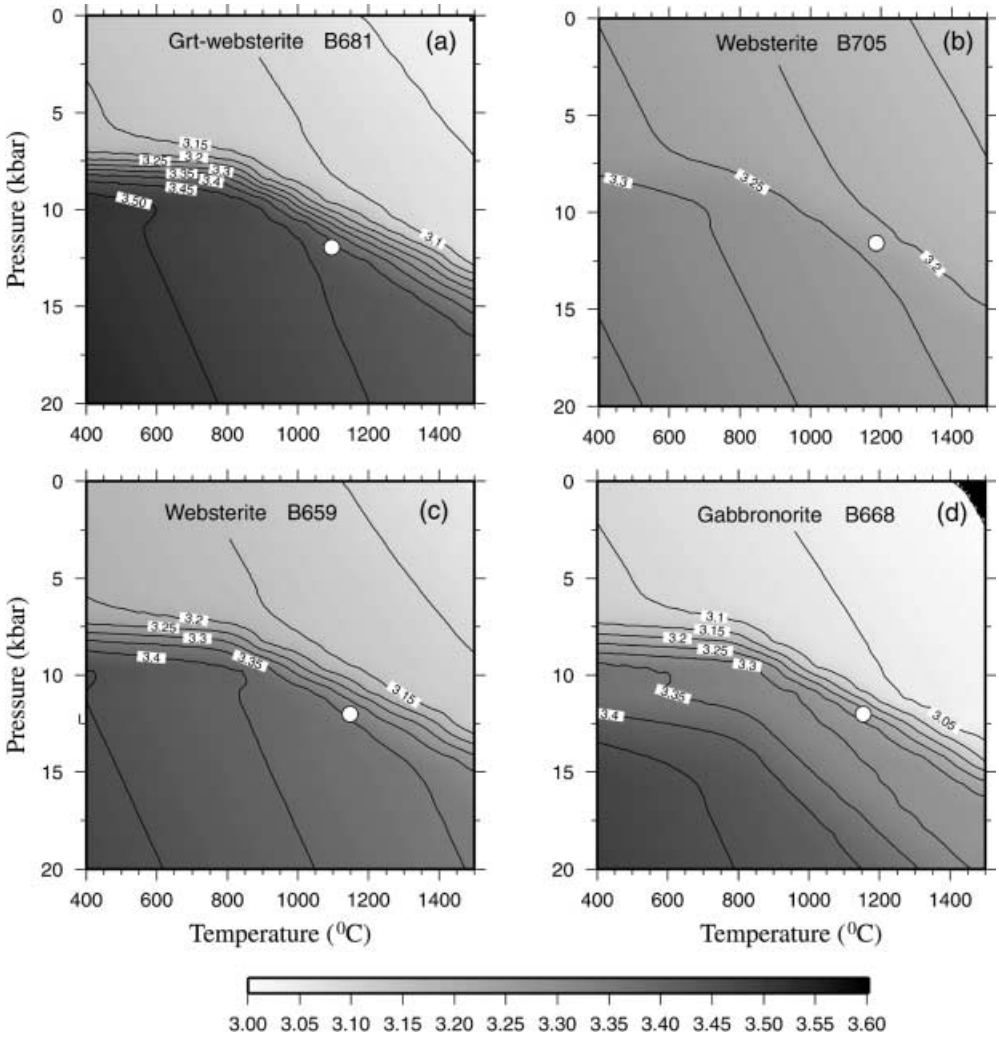

Fig. 8 Calculated densities (g/cm^3) for experimental solid compositions listed in Table 4. Subsolidus phase assemblages and densities were calculated with Vertex (Connolly 1990) with the database of Holland and Powell (1998) using an interface and plotting software developed by M. Jull at Woods Hole. Phase assemblages were calculated at P and T down to 800 °C, and then densities for lower temperatures using the phase assemblages at (P, 800 °C) and the compressibility of the minerals. *Circles* indicate experimental conditions as listed in Table 2

stabilized earlier effecting a decreasing or negative density contrast between plagioclase bearing cumulates and peridotite (Fig. 9d). It appears that there is a critical H_2O content and temperature range that optimizes the density contrast between ultramafic plutonic rocks and the upper mantle. For the compositions we studied, the density contrast between ultramafic plutonic rocks and peridotite is largest if the primary liquid contains about 3.5 wt% H_2O and is garnet saturated (at temperatures less than about 1,100 °C).

Igneous pyroxenites and the genesis of continental crust

Clinopyroxene compositions from websterites at the base of arc crustal sections generally have Mg# >0.85, Cr_2O_3 contents >0.4 wt% and surprisingly low Al_2O_3 (<3 wt%, but often <2 wt%; (DeBari and Coleman 1989; Gravestock 1992; Jan and Howie 1981). Clearly these pyroxenites crystallized from primitive mantle melts, because Cr is highly compatible and decreases rapidly in concentration during crystallization. However, many websterites are olivine-free, whereas any melt multiply saturated with a peridotite assemblage at a relatively high pressure will first crystallize olivine at lower pressures (e.g., Kushiro and Yoder 1966; O'Hara 1968). In order to crystallize high Mg#, olivine-free websterite, the primary magma has to be a relatively Si-rich melt which has a limited interval of olivine crystallization, because fractionation of significant proportions of olivine would decrease the Mg# of the derivative liquid and resulting pyroxenites. The olivine crystallization interval is smallest at pressures close to the multiple saturation point of a respective composition. We can thus infer that the magmas, which formed olivine-free pyroxenites at the base of arc crust, were saturated in mantle peridotite compositions at only slightly greater depth.

Olivine addition experiments were performed to investigate the extent of the olivine crystallization interval in our experimental basalt composition (Table 2). In the basalt composition, the crystallization assemblage changes from olivine alone to olivine and two pyroxenes within a temperature interval of only 40 °C. This indicates that the temperature window of olivine

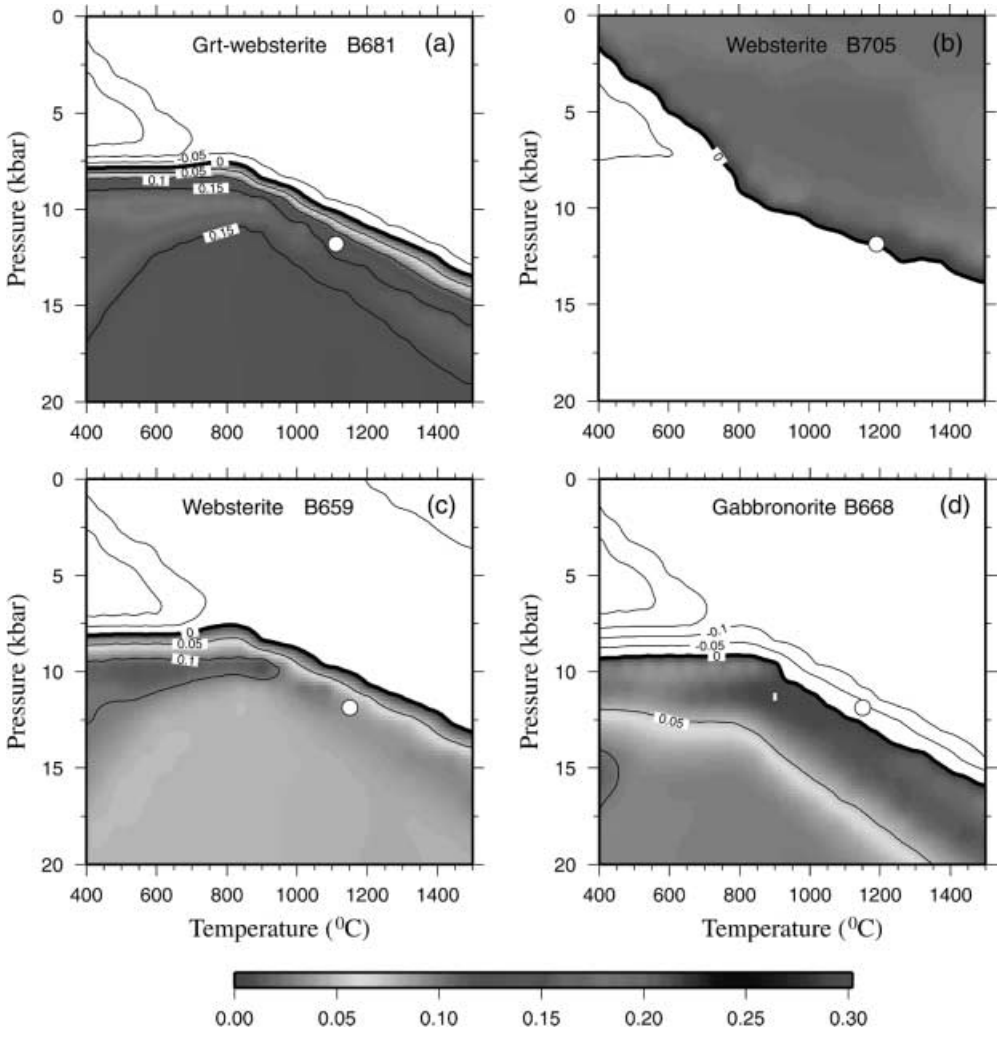

Fig. 9 Calculated density difference (g/cm^3) between experimental solid compositions and abyssal peridotite (Dick 1989). The *shaded region* indicates pressure-temperature conditions at which plutonic cumulates are denser than the underlying mantle

crystallization at lower crustal pressures can be small, and that olivine-free, high Mg# websterite might form by peritectic reactions of the type olivine + liquid → pyroxene. Parman (personal communication, 2000) has performed similar experiments on the magnesian andesite composition and reached the same result. This result is expected since both compositions are high Mg# near-primary hydrous melts of the mantle wedge (Baker et al. 1994).

Recently, Burg et al. (1998) has interpreted websterite rocks from the Jijal complex in Kohistan to be the result of metasomatic replacement of uppermost mantle rocks. Their arguments were based mainly on the observation that relict dunites ('flames, streaks') are enclosed in websterites. Dunites enclosed in websterite have also been observed by Girardeau et al. (1989) from the Cabo Ortegal pyroxenite complex. Based on our experimental data, we think that dunites and olivine-free websterite cumulates may form by repeated intrusions of primitive, Si-rich magmas, and that the relic dunites can be explained by incomplete peritectic reactions similar to those obtained by the olivine-addition experiments.

In the Kohistan arc crustal section, amphibole pyroxenites and garnet-amphibole pyroxenites overlie websterites (Miller and Christensen 1994; Burg et al. 1998). Above these, plagioclase appears in gabbronorites with pyroxene Mg# of about 0.8. This field sequence is similar to the experimental solid assemblages produced over a temperature interval beginning above 1,100–1050 °C. It is therefore likely that the Kohistan ultramafic plutonic rocks crystallized from hydrous magmas with several wt% H_2O, in which plagioclase crystallization was suppressed and only occurred in evolved liquid (e.g.. Mg# in pyroxenes < 0.8).

In exposed arc terranes such as Tonsina and Kohistan, a sharp transition exists as marked by the first occurrence of plagioclase in ultramafic rocks and abundant gabbros, covering over tens to several hundred meters (e.g., (DeBari and Coleman 1989; Miller and Christensen 1994). As physical properties such as density and P-wave velocity of plagioclase-bearing rocks are quite different from those of ultramafic plutonic rocks (Miller and Christensen 1994), the plagioclase saturation boundary in igneous crust will produce a sharp Moho on seismic profiles (e.g., Kushiro 1990; Miller and

Christensen 1994). Thus, any estimate of the composition of the continental crust must take ultramafic cumulates into account which seismically resemble residual mantle peridotite, but genetically 'belong' to the igneous crust.

Our experiments show that up to 50% of primary, mantle-derived liquid could crystallize as ultramafic plutonic rocks before plagioclase saturation occurs. Conrad and Kay (1984) calculated that primitive mantle-derived magmas form 21% ultramafic cumulates below the Moho. However, such estimates are dependent on the crystallization pressure and the H_2O content of primary liquids.

Estimation of the volume of ultramafic plutonic rocks has direct implications on estimates of the composition of the continental crust. Estimates of the composition of the continental crust (e.g., Christensen and Mooney 1995; Kelemen 1995; Rudnick and Fountain 1995) yield high Mg# andesite to dacite compositions (molar Mg# from 0.45 to 0.57, wt% SiO_2 from 57 to 65). In contrast, calculations from arcs (DeBari and Sleep 1991; Miller and Christensen 1994) are significantly more mafic. To explain this paradox several models have been proposed (see Rudnick 1995: Kelemen 1995, for a review): (1) present-day arc magmatism is not the major crust-forming process, and instead continental growth was mainly in the Archean when mantle temperatures where higher and melting of mafic crust was widespread; (2) the average melt flux from the mantle to form crust at various times and places has been 'andesitic', not 'basaltic'; (3) calculations of the continental crust underestimate the mass of ultramafic plutonic rocks and therefore result in an andesitic composition, and (4) that a ''delamination'' process removes dense, mafic plutonic rocks and cycles them back into the mantle.

Based on our experimental results and density calculations, we suggest that a combination of mechanisms (2), (3), and (4) might be important in explaining the bulk composition of the continental crust.

With regard to mechanism (2), in which mantle-derived magmas are predominantly andesitic at various times and places, our results indicate that the primitive high MgO basalt and high Mg# andesite used for this experimental investigation are permissive parental magma compositions that could undergo fractional crystallization at the base of the crust to produce pyroxene-rich cumulates. Furthermore, low aluminum pyroxenites at the base of the Talkeetna, and Kohistan arc crustal sections formed by crystallization of mantle-derived orthopyroxene-saturated liquids with high Si/Al. Thus, although the bulk composition of the Talkeetna and Kohistan sections has been estimated to be basaltic (DeBari and Sleep 1991; Miller and Christensen 1994), it is now apparent that these compositions must be mixtures of rocks formed by crystallization of andesitic as well as basaltic primary liquids.

A recent dynamical study by Jull and Kelemen (2001) concluded that mechanism (4), delamination of two distinct types of dense, lower crustal igneous rocks is likely in regions with Moho temperatures greater than about 700 °C that are sustained for more than 10 million years. Jull and Kelemen (2001) found that the two rock types most likely to be unstable are ultramafic cumulates – which are denser than residual mantle peridotite at almost any pressure and temperature because they have no plagioclase and always have higher Fe/Mg than residual peridotite – and garnet granulites. (Eclogites would also be denser than the underlying mantle, but form only at the base of anomalously thick crust, or at temperatures less than 700 °C where high viscosities make delamination unlikely).

Formation of ultramafic plutonic rocks is known to occur in arcs, based on both phase equilibrium of hydrous, primitive magmas and observations from exposed arc crustal sections, zoned ultramafic plutons, and xenoliths. It is also apparent that Moho temperatures are very high in arcs, in excess of 1,000 °C (e.g., Blackwell et al. 1982; Zhao et al. 1992). At temperatures greater than 1,000 °C, Jull and Kelemen (2001) found that a 10-km-thick ultramafic cumulate layer at the base of the crust would delaminate in less than 1 million years. Under appropriate conditions, for example in the temperature range of 1,300–1,100 °C or in the presence of a background tectonic strain rate, even layers less than 1 km thick could become unstable in the same period of time. Thus, one can envision a near steady-state process in which ultramafic cumulates are produced and then returned to the mantle, leading to a divergence between the composition of continental crust and that of primitive, mantle-derived magmas.

Mechanism (3) may also play a role if previous estimates of continental crust composition underestimated the volume of ultramafic plutonic rocks. For example, recent 3D seismic studies of the western Sierra Nevada indicate that some regions beneath the Moho have low P-wave velocities which may be caused by significant amounts of pyroxenitic material (Fliedner et al. 2000). Such an interpretation is partially supported by xenoliths studies of Ducea and coworkers (Ducea and Saleeby 1996; 1998). On the other hand, the majority of the ultramafic xenoliths of the western US are residual peridotite, as indicated by the compilation of Wilshire et al. (1988). Also, the pyroxenite layers at the base of the Kohistan and Talkeetna arc sections and overlying residual mantle harzburgite and underlying plagioclase-bearing plutonic rocks, (less than 1 km thick), comprise less than 3% of the original crustal thickness of about 35 km estimated from geobarometry (DeBari and Coleman 1989; Miller and Christensen 1994).

In addition, while estimated continental crust has surprisingly low Al_2O_3 (about 16 wt%), crystallization of ultramafic cumulates leads to formation of increasingly Al-rich derivative liquids. Thus, if the seismically defined (plagioclase-bearing) continental crust were produced by extensive crystallization of ultramafic cumulates from a mantle-derived melt with an initial Al_2O_3 content of about 16 wt% (similar to mantle-derived

MORB; e.g., Kinzler 1997) the crust would have a significantly higher Al_2O_3 concentration than is currently estimated. This casts doubt on the possible significance of mechanisms (3) and (4). Alternatively, perhaps mantle melts parental to continental crust had substantially less than 16 wt% Al_2O_3.

Clearly, mechanisms (3) and (4) require further investigation. As Fliedner et al. (2000) pointed out, seismic anisotropy studies might be an approach to differentiate between residual peridotites and ultramafic plutonic rocks.

Conclusions

We have documented the effects of H_2O and composition on the crystallization of primitive magmas corresponding to conditions at the base of arc crust. We find that some aspects of exposed pyroxenite and related ultramafic plutonic rocks in arcs can be explained by crystallization of hydrous magmas at a pressure of 1.2 GPa. Small variations in the amount of H_2O in the liquid have large effects on the crystallization sequence. At high pressures relevant to the deep arc crust, SiO_2-poor phases such as amphibole and garnet crystallize before plagioclase and drive derivative liquids to corundum-normative, calc-alkaline compositions, a feature which has been reported for about 15% of erupted andesites (Gill 1981). Thus, assimilation of pelitic material is not required for the generation of peraluminous liquids in arcs.

Density calculations for the experimental solid assemblages indicate that ultramafic plutonic rocks at the base of arc crust have densities exceeding those of residual mantle peridotite by 0.05 to 0.20 g/cm^3. The largest density difference results for the solid assemblages crystallized from liquids with intermediate H_2O contents (ca. 3.5 wt%) at less than about 1,100 °C, which included garnet but no plagioclase.

The seismic Moho in most arcs probably corresponds to the plagioclase-saturation boundary. However, the combined effects of high total pressure and high H_2O contents in magmas at the base of arc crust will suppress plagioclase until significant amounts of the initial magma mass is crystallized, possibly up to 60%. This has the interesting consequence that the seismic Moho and the transition from igneous crust to residual mantle peridotite nearly coincide underneath shallow oceanic crust (dry, low pressure crystallization), whereas in subduction-related magmatic arcs the seismic Moho may be significantly shallower than the igneous crust – residual mantle transition (wet, high pressure crystallization).

Acknowledgements This research was support by a Swiss NSF/WHOI postdoctoral fellowship to OM, by NSF research grants OCE-9416616 and EAR-9814632 to PBK, and by research grant EAR-9706214 to TLG. We thank Matthew Jull for his help with the density calculations, and Greg Hirth, Steve Parman, Jim van Orman and Roberta Rudnick for discussions. Peter Ulmer and Stefano Poli provided very helpful reviews.

References

Baker MB, Grove TL, Price R (1994) Primitive basalts and andesites from the Mt. Shasta region, N. California: products of varying melt fraction and water content. Contrib Mineral Petrol 118:111–129

Bartels KS, Kinzler RJ, Grove TL (1991) High pressure phase relations of primitive high-alumina basalts from Medicine Lake volcano, northern California. Contrib Mineral Petrol 108:253–270

Blackwell DD, Bowen RG, Hull DA, Riccio J, Steele JL (1982) Heat flow, arc volcanism, and subduction in northern Oregon. J Geophys Res 87:8735–8754

Boyd FR, England JL (1960) Apparatus for phase equilibrium measurements of pressures up to 50 kbars and temperatures up to 1750 °C. J Geophys Res 65:741–748

Burg JP, Bodinier JL, Chaudhry S, Hussain S, Dawood H (1998) Infra-arc mantle-crust transition and intra-arc mantle diapirs in the Kohistan complex (Pakistani Himalaya): petro-structural evidence. Terra Nova 10:74–80

Cawthorn RG, Brown PA (1976) A model for the formation and crystallization of corundum-normative calcalkaline magmas through amphibole fractionation. J Geol 84:467–476

Christensen NI, Mooney WD (1995) Seismic velocity structure and composition of the continental crust: a global view. J Geophys Res 100:9761–9788

Connolly JAD (1990) Multivariable phase diagrams: an algorithm based on generalized thermodynamics. Am J Sci 290:666–718

Conrad WK, Kay RW (1984) Ultramafic and mafic inclusions from Adak Island: crystallization history and implications for the nature of primary magmas and crustal evolution in the Aleutian island arc. J Petrol 25:88–125

DeBari SM, Coleman RG (1989) Examination of the deep levels of an island arc: evidence from the Tonsina ultramafic-mafic assemblage, Tonsina, Alaska. J Geophys Res 94:4373–4391

DeBari SM, Sleep NH (1991) High-Mg, low-Al bulk composition of the Talkeetna island arc, Alaska: implications for primary magmas and the nature of arc crust. Geol Soc Am Bull 103: 37–47

Dick HJB (1989). Abyssal peridotites, very slow spreading ridges and ocean ridge magmatism. In: Saunders AD, Norry MJ (eds) Magmatism in the ocean basins. Geol Soc Spec Publ 42:71–105

Draper DS, Johnston AD (1992) Anhydrous PT Phase Relations of an Aleutian high-MgO Basalt: an investigation of the role of olivine-liquid reaction in the generation of high-alumina basalts. Contrib Mineral Petrol 112:501–519

Ducea MN, Saleeby JB (1996) Buoyancy sources for a large, unrooted mountain range, the Sierra Nevada, California: Evidence form xenolith thermobarometry. J Geophys Res 101:8229–8244

Ducea MN, Saleeby JB (1998) The age and origin of a thick mafic-ultramafic keel from beneath the Sierra Nevada batholith. Contrib Mineral Petrol 133:169–185

Fliedner MM, Klemperer SL, Christensen NI (2000) Three-dimensional seismic model of the Sierra Nevada arc, California, and its implications for crustal and upper mantle composition. J Geophys Res 105:10899–10921

Gaetani GA, Grove TL (1995) Partitioning of rare earth elements between clinopyroxene and silicate melt: crystal-chemical controls. Geochim Cosmochim Acta 59:1951–1962

Gaetani GA, Grove TL (1998) The influence of water on melting of mantle peridotite. Contrib Mineral Petrol 131:323–346

Gaetani GA, Grove TL, Bryan WB (1993) The influence of water on the petrogenesis of subduction-related igneous rocks. Nature 365:332–334

Gill JB (1981) Orogenic andesites and plate tectonics. Springer, Berlin Heidelberg New York

Girardeau J, Gil Ibarguchi JI, Ben Jamaa N (1989) Evidence for a heterogeneous upper mantle in the Cabo Ortegal complex, Spain. Science 245:1231–1233

Gravestock PJ (1992) The chemical causes of uppermost mantle heterogeneities. PhD Thesis, The Open University

Grove TL, Baker MB (1984) Phase equilibrium controls on the tholeiitic versus calc-alkaline differentiation trends. J Geophys Res 89:3253–3274

Grove TL, Gerlach DC, Sando TW (1982) Origin of calc-alkaline series lavas at Medicine Lake Volcano by fractionation, assimilation and mixing. Contrib Mineral Petrol 80:160–182

Grove TL, Kinzler RJ, Bryan WB, (1993) Fractionation of mid-ocean ridge basalt (MORB). In: Phipps Morgan J, Blackman DK, Sinton JM (eds) Mantle flow and melt generation at mid-ocean ridges. Geophysical Monograph. American Geophysical Union, Washington, DC, pp 281–310

Grove TL, Kinzler RJ (1986) Petrogenesis of andesites. Ann Rev Earth Planet Sci 14:417–454

Hays JF (1966) Lime-alumina-silica. Carnegie Inst Wash Yearbook 65:234–239

Helz RT (1973) Phase relations of basalts in their melting range at P_{H2O} = 5 kbar as a function of oxygen fugacity. Part I. Mafic phases. J Petrol 14:249–302

Hirose K, Kawamoto T (1995) Hydrous partial melting of lherzolite at 1 GPa: The effect of H_2O on the genesis of basaltic magmas. Earth Planet Sci Lett 133:463–473

Holland TJB, Powell R (1998) An internally consistent thermodynamic data set for phases of petrological interest. J Metamorphic Geol 16:309–343

Holloway JR, Burnham CW (1972) Melting relations of basalt with equilibrium water pressure less than total pressure. J Petrol 13:1–29

Jan MQ, Howie RA (1981) The mineralogy and geochemistry of the metamorphosed basic and ultrabasic rocks of the Jijal complex, Kohistan, NW Pakistan. J Petrol 22:85–126

Jull M, Kelemen PB (2001) On the conditions for lower crustal convective instability. J Geophys Res: in press

Kelemen PB (1986) Assimilation of ultramafic rocks in subduction-related magmatic arcs. J Geol 94:829–843

Kelemen PB (1995) Genesis of high Mg# andesites and the continental crust. Contrib Mineral Petrol 120:1–19

Kelemen PB, Ghiorso MS (1986) Assimilation of peridotite in zoned calc-alkaline plutonic complexes: evidence from the Big Jim Complex, Washington Cascades. Contrib Mineral Petrol 94:12–28

Kelemen PB, Joyce DB, Webster JD, Holloway JR (1990) Reaction between ultramafic rock and fractionating basaltic magma II. Experimental investigation of reaction between olivine tholeiite and harzburgite at 1150–1050 °C and 5kbar. J Petrol 31:99–134

Kinzler RJ (1997) Melting of mantle peridotite at pressures approaching the spinel to garnet transition: application to mid-ocean-ridge basalt petrogenesis. J Geophys Res 102:853–874

Kinzler RJ, Grove TL (1992) Primary magmas of mid-ocean ridge basalts 1. Experiments and methods. J Geophys Res 97:6885–6906

Kress VC, Carmichael ISE (1991) The compressibility of silicate liquids containing Fe_2O_3 and the effect of composition, temperature, oxygen fugacity and pressure on their redox states. Contrib Mineral Petrol 108:82–92

Kushiro I (1990) Partial melting of mantle wedge and evolution of usland arc crust. J Geophys Res 95:15,929–15,939

Kushiro I, Yoder HS (1966) Anorthite-forsterite and anorthite-enstatite reactions and their bearing on the basalt-eclogite transformation. J Petrol 7: 337–362

Kushiro I, Yoder HS (1972) Origin of calc-alkalic peraluminous andesite and dacites. Carnegie Inst Wash Yearbook 71:411–413

Miller DJ, Christensen NI (1994) Seismic signature and geochemistry of an island arc: a multidisciplinary study of the Kohistan accreted terrane, northern Pakistan. J Geophys Res 99:11623–11642

O'Hara MJ (1968) The bearing of phase equilibria studies on the origin and evolution of basic and ultrabasic rocks. Earth Sci Rev 4:69–133

Robinson JAC, Wood BJ, Blundy JD (1998) The beginning of melting of fertile and depleted peridotite at 1.5 GPa. Earth Planet Sci Lett 155:97–111

Rudnick RL (1995) Making continental crust. Nature 378:571–577

Rudnick RL, Fountain DM (1995) Nature and composition of the continental crust: a lower crustal perspective. Rev Geophys 33:267–309

Sautter V, Jaoul O, Abel F (1988) Aluminum diffusion in diopside using the $^{27}Al(p, \gamma)^{28}Si$ nuclear reaction: preliminary results. Earth Planet Sci Lett 89:109–114

Sisson TW, Grove TL (1993a) Experimental investigations of the role of H_2O in calc-alkaline differentiation and subduction zone magmatism. Contrib Mineral Petrol 113:143–166

Sisson TW, Grove TL (1993b) Temperatures and H_2O contents of low-MgO high-alumina basalts. Contrib Mineral Petrol 113:167–184

Taylor SR, McLennan SM (1985) The continental crust: its composition and evolution. Blackwell, Oxford

Wilshire HG, Meyer CE, Nakata JK, Calk LC, Shervais JW, Nielson JE, Schwarzman EC (1988) Mafic and ultramafic xenoliths from volcanic rocks of the western United States. USGS Prof Pap 1443:1–179

Zhao D, Hasegawa A, Horiuchi S (1992) Tomographic imaging of P and S wave velocity structure beneath northeastern Japan. J Geophys Res 97:19909–19928